# In situ chemical composition measurement of individual cloud residue particles at a mountain site, South China

Qinhao Lin[1,2], Guohua Zhang[1], Long Peng[1,2], Xinhui Bi[1,*], Xinming Wang[1], Fred J. Brechtel[3], Mei Li[4], Duohong Chen[5], Ping'an Peng[1], Guoying Sheng[1], Zhen Zhou[4]

[1] State Key Laboratory of Organic Geochemistry and Guangdong Key Laboratory of Environmental Protection and Resources Utilization, Guangzhou Institute of Geochemistry, Chinese Academy of Sciences, Guangzhou, 510640, PR China

[2] University of Chinese Academy of Sciences, Beijing, 100049, PR China

[3] Brechtel Manufacturing Inc., Hayward, 94544, California, USA

[4] Atmospheric Environment Institute of Safety and Pollution Control, Jinan University, Guangzhou 510632, PR China

[5] State Environmental Protection Key Laboratory of Regional Air Quality Monitoring, Guangdong Environmental Monitoring Center, Guangzhou 510308, PR China

* Correspondence to: Xinhui Bi (bixh@gig.ac.cn)

Tel.: +86-20-85290195

## Highlights

1. EC-containing particles comprised the largest fraction of the total cloud residues (49.3% by number), with dominating size 0.2-1.0 μm.

2. Amine particles represented 0.2% to 15.1% by number of the total cloud residues dependent on the air mass history, with dominating size 0.7-1.9 μm.

3. Higher fraction, intensity (average ion peak area) and larger size of nitrate-containing particles were found in the cloud residues relative to the ambient particles.

## Abstract

To estimate how atmospheric aerosol particles interact with chemical composition of cloud droplets, a ground-based counterflow virtual impactor (GCVI) coupled with a real-time single-particle aerosol mass spectrometer (SPAMS) was used to assess the chemical composition and mixing state of individual cloud residue particles in the Nanling Mountain Range (1,690 m a.s.l.), South China, in Jan 2016. The cloud residues were classified into nine particle types: Aged elemental carbon (EC), Potassium-rich (K-rich), Amine, Dust, Pb, Fe, Organic carbon (OC), Sodium-rich (Na-rich) and Other. The largest fraction of the total cloud residues was the aged EC type (49.3% by number), followed by the K-rich type (33.9% by number). Abundant aged EC cloud residues that internally mixed with inorganic salts were found in air masses from northerly polluted areas. The number fraction (Nf) of the K-rich cloud residues increased within southwesterly air masses from fire activities in Southeast Asia. In addition, the Amine particles increased from 0.2% to 15.1% by number to the total cloud residues, when air masses changed from northerly polluted areas to southwesterly ocean and livestock areas. The Dust, Fe, Pb, Na-rich and OC particles had a low contribution (0.5-4.1% by number) to the total cloud residues. Higher fraction of nitrate (88-89% by number) was found in the Dust and Na-rich cloud residues relative to sulfate (41-42%) and ammonium (15-23%). Higher fraction, intensity (average ion peak area) and larger size of nitrate-containing particles were found in the cloud residues relative to the ambient particles. To our knowledge, this study is the first report on in situ observation of the chemical composition and mixing state of individual cloud residue particles in China. This study increases our understanding of the impacts of aerosols on cloud droplets in a remote area of China.

Keywords: GCVI, SPAMS, cloud residues, mixing state, South China

## 1 Introduction

Aerosol-cloud interactions influence the thermodynamic and radiation balance of the atmosphere (IPCC, Boucher et al., 2013). Anthropogenic particles can increase number concentration of small cloud droplets, in turn, affect reflectivity and life time of clouds (Stier et al., 2005; Lohmann et al., 2007; Rosenfeld et al., 2008). In-situ cloud chemical measurements show varied chemical composition of cloud water or residues at various regions (Sorooshian et al., 2007a; Roth et al., 2016; Li et al., 2017). Although a large number of aerosol/cloud studies over the past 20 years, the uncertainty for evaluating radiative forcing due to aerosol-cloud interactions has not been reduced (Seinfeld. et al., 2016). Therefore, it is crucial to assess how atmospheric aerosol particles contribute and interact with cloud droplets.

The formation of cloud condensation nuclei (CCN) is dependent on the size and chemical composition of atmospheric aerosol particles at a given supersaturation (McFiggans et al., 2006). A change in the chemical composition of atmospheric aerosol particles during atmospheric aging processes can strongly alter their CCN ability. The presence of hydrophobic surface films lowers the CCN ability of atmospheric aerosol particles (Andreae and Rosenfeld, 2008). Elemental carbon (EC) particles, normally considered insoluble, show high CCN activity after mixing with sulfuric acid (Zhang et al., 2008). However, sulfate and nitrate, which are generally regarded as soluble materials, were found in particles ranging from high to low hygroscopicity (Herich et al., 2008).

Furthermore, several cloud measurements have pointed to a lower number fraction (Nf) or mass fraction of sulfate-containing particles in cloud droplets relative to ambient or interstitial particles (Drewnick et al., 2007; Twohy and Anderson, 2008). On the contrary, other studies have reported a larger Nf of sulfate-containing particles in cloud droplets (Zelenyuk et al., 2010; Roth et al., 2016). These discrepancies suggest that the influence of the mixing state of atmospheric aerosol particles on CCN activity remains unclear.

The combined technique of a counterflow virtual impactor (CVI) and Aerosol Mass Spectrometer (AMS) or single-particle measurement is widely used to characterize the chemical composition and mixing state of cloud/fog droplet residue particles. These studies were mainly conducted in North America including Wyoming (Pratt et al., 2010a), Ohio (Hayden et al., 2008), Oklahoma (Berg et al., 2009), Florida (Cziczo et al., 2004; Twohy et al., 2005), California (Coggon et al., 2014), Europe including Schmücke (Roth et al., 2016; Schneider et al., 2017), Jungfraujoch (Kamphus et al., 2010), Åreskutan (Drewnick et al., 2007), Scandinavia (Targino et al., 2006), Arctic (Zelenyuk et al., 2010), Central America (Cziczo et al., 2013), West Africa (Matsuki et al., 2010) and Oceans (Twohy and Anderson 2008; Twohy et al., 2009; Shingler et al., 2012). Over the past three decades, China has undergone rapid economic growth accompanied by increased aerosol emissions. Scientists have worked to increase our understanding of an emissions inventory and the temporal and spatial variation of atmospheric aerosols in China (Zhang et al., 2012b). However, few studies employ direct observation of the chemical composition and mixing state of cloud/fog droplets. Li et al. (2011b) used transmission electron microscopy to obtain mixing state of single ambient particle during cloud events at Mt. Tai in northern China. Their result showed that sulfate-related salts dominated in large particle. Bi et al.

(2016) used a ground-counterflow virtual impactor (GCVI) coupled with a real-time single particle aerosol mass spectrometer (SPAMS) to explore the chemical composition and mixing state of single fog residue particles in an urban area of South China at ground level. They found abundant anthropogenic emitted particles including soot or element carbon (EC) in fog residues.

Here, we present a study on the chemical composition and mixing state of individual cloud residue particles at a mountain site of South China. The same experimental methods of Bi et al. (2016) were used in this study on the summit of South China's Nanling mountain region. The size distribution, chemical composition and mixing state of cloud residues during cloud events are discussed. Moreover, the chemical compositions of ambient and non-activated particles were also compared with the cloud residues. The aim of this study is to assess the potential effects of anthropogenic aerosols from regional transportation on cloud formation and to investigate the dominant particle types in cloud droplets at a mountain site in South China.

## 2 Experimental

### 2.1 Measurement site

Measurements were carried out 15-26 Jan, 2016. The sampling site was located in the Nanling Background Station (112 °53' 56" E, 24° 41' 56" N, 1,690 m a.s.l.) at the National Air Pollution Monitoring System in South China (Figure S1). This station is 200 km north of the metropolitan city Guangzhou and 350 km north of the South China Sea. This site is also surrounded by a national park forest (273 km$^2$) where there are hardly any emissions from anthropogenic activities. However, during the winter monsoon period, air pollution from northern China moves south to the southern coastal region and crosses the study region (Lee et al., 2005).

## 2.2 Instrumentation

In this study, a GCVI inlet system (GCVI Model 1205, Brechtel Mfg. Inc.) was used to sample cloud droplets with a diameter greater than 8 μm. Ambient temperature on average was 6.9 ℃ (ranging from -7.2 to 11.4 ℃) during cloud events in this study. Therefore, the clouds here consisted of liquid droplets only. Measurement of drop size spectrum in this region performed during winter of 1999-2001 shows that size of cloud droplets ranged from 4 to 25 μm, with average size of 10 μm and a corresponding liquid water content of 0.11-0.15 g $m^{-3}$ (Deng et al., 2007). Some studies in other locations also showed an average size at ~10 μm (Freud et al., 2008; Shingler et al., 2012). Therefore, it is reasonable to select a cut size at 8 μm for cloud droplets in the present study. The sampled cloud droplets were passed through an evaporation chamber (air flow temperature at 40 ℃), where the associated water was removed and the dry residue particles (with the air flow RH lower than 30%), considered as CCN, remained. The particle transmission efficiency of the cut size (8 μm) was 50% (Shingler et al., 2012). The enrichment factor of the particles collected by the GCVI inlet was estimated to be 5.25 based on theoretical calculation (Shingler et al., 2012). Ambient particles were collected through an ambient inlet with a cut-off aerodynamic diameter ($d_a$) of 2.5 μm when no cloud events were present. Additionally, non-activated particles were sampled through the ambient inlet during the cloud events. The cloud droplet residues, ambient or non-activated particles were subsequently analyzed by a suite of aerosol measurement devices, including a SPAMS (Hexin Analytical

Instrument Co., Ltd., Guangzhou, China), a scanning mobility particle sizer (SMPS) (MSP Cooperation) and an aethalometer (AE-33, Magee Scientific Inc.). Detailed information and parameter settings regarding the GCVI operation can be found in the work of Bi et al. (2016).

A detailed operational principle of the SPAMS has been described elsewhere (Li et al., 2011a). Briefly, aerosol particles are drawn into SPAMS through a critical orifice. The particles are focused and aerodynamically sized by two continuous diode Nd:YAG laser beams (532 nm). The particles are subsequently desorbed/ionized by a pulsed laser (266 nm) triggered exactly based on the velocity of the specific particle. The positive and negative ions generated are recorded with the corresponding size of each singe particle. Polystyrene latex spheres (Nanosphere Size Standards, Duke Scientific Corp., Palo Alto) of 0.2-2.0 μm in diameter were used to calibrate the sizes of the detected particles on the mountain top station. The ambient pressure was 830 hPa (826-842 hPa) during the measurements and during the calibration. Particles measured by SPAMS mostly fell within the size range of $d_{va}$ 0.2-2.0 μm (Li et al., 2011a).

## 2.3 Definition of cloud events

To reliably identify the presence of cloud events, an upper-limit visibility threshold of 5 km and a lower-limit relative humidity (RH) threshold of 95% were set in the GCVI software (Bi et al., 2016). Three long-time cloud events occurred during the periods of 16:00 (local time) 15 Jan - 07:00 17 Jan (cloud I), 20:00 18 Jan - 12:00 19 Jan (cloud II) and 17:00 19 Jan - 13:00 23 Jan (cloud III), as marked in Figure 1. In addition, a cloud event occurred at 14:40 - 15:00 on 17 Jan, but we did not complete an analysis due to the short duration of this cloud event. The measured cloud residual concentration was integrated by a SMPS and was divided by 5.25 (enrichment factor of CVI). The corrected cloud residual concentrations on average were 218 $cm^{-3}$, 284 $cm^{-3}$ and 272 $cm^{-3}$ for cloud I, cloud II and cloud III, respectively (Figure S2). Note that during cloud events, ambient RH was close to 100%, as illustrated in Figure 1. Low level of PM2.5 (~ 12.7 μg $m^{-3}$) excludes the influence of hazy days. A rainfall detector of the GCVI system was also used to exclude rain droplet contamination. When cloud events occurred without precipitation, sampling was automatically triggered by the GCVI control software.

## 2.4 Particle classification

During the study period, a total of 73996 sampled particles including 49322 ambient, 23611 cloud residues and 1063 non-activated particles with bipolar mass spectra were chemically analyzed in the size range of $d_{va}$ 0.2-1.9 μm. The sampled particles were first classified into 101 clusters using an Adaptive Resonance Theory neural network (ART-2a) with a vigilance factor of 0.75, a learning rate of 0.05, and 20 iterations (Song et al., 1999). By manually combining similar clusters, aged EC, Potassium-rich (K-rich), Amine, Dust, Fe, Pb, Organic carbon (OC), and Sodium-rich (Na-rich), eight major particle types with distinct chemical patterns were obtained, which represented ~99.9% of the population of the detected particles. The remaining particles were grouped together as "Other". Assuming that number of individual particles follows Poisson distribution, standard errors for number fraction of particle type were estimated (Pratt et al., 2010a).

## 3 Results and discussion

### 3.1 Back trajectories and meteorological conditions

Back trajectories in this study were calculated using the Hybrid Single Particle Lagrangian Integrated Trajectory (HYSPLIT Model). Heights of the HYSPLIT model in the study region (a spatial resolution of 0.5 ° × 0.5 °) is averaged 500 m a.s.l., lower than height of the observed site (1,690 m a.s.l.). Therefore, a height of 1,800 m a.s.l. (approximately 100 m above the observed site) was chosen as an endpoint in the model. During the study period, the station was mainly affected by southwesterly or northerly air masses (Figure 2). In addition, the beginning of southwesterly air masses traversed at lower heights relative to northerly air masses (Figure 2). The southwesterly air masses, accompanied by warm and moist airflows, occurred during 15-17 and 20-21 Jan, which promoted cloud formation (Figure 1). Conversely, the northerly air masses, associated with cool and dry airstreams, occurred during 18 and 23-24 Jan and led to a decrease in temperature and relative humidity. Note that on 18-19 and 22-23 Jan, the air mass encountered initial mixing of northerly cloud-free air and southwesterly cloudy air. Entrained of nuclei particles originated from northern air mass would be activated to become cloud droplets (Sect. 3.4). On the other hand, entrainment of non-activated particles originated from northern air mass has also mixed into the cloud (Sect. 3.5).

Meteorological conditions were unstable, with high southwesterly flow (~ 6.5 m $s^{-1}$) during 15-17 and 20-22 Jan (Figure 1). The level of $PM_{2.5}$ remained low with a value of approximately 3 μg $m^{-3}$ for this time period. A high level of $PM_{2.5}$ (~20 μg $m^{-3}$) was observed during 18 Jan when the northerly flow dominated. Similarly, the average $PM_{2.5}$ value reached 24 μg $m^{-3}$ during 24 Jan when the local northerly and southwesterly flows occurred alternately. However, the particles still originated from northerly air masses for this period (Figure 2). During 23-24 Jan, a big freeze associated with a violent northerly flow and a wind speed that exceeded the upper-limit speed (~12 m/s) of a wind speed sensor resulted in a sharp decrease in temperature (Figure 1).

### 3.2 The chemical characterization of cloud droplet residues

Figure 3 shows the average positive and negative mass spectra of main six particle types. The aged EC particles were identified by EC cluster ions (e.g., m/z $\pm 12C^{+/-}$, $\pm 36C_3^{+/-}$, $\pm 48C_4^{+/-}$, $\pm 60C_5^{+/-}$, …) and a strong $K^+$ ion signal (m/z $39K^+$) as well as a sulfate ion signal (m/z $-97HSO_4^-$), and minor organic markers (m/z $27C_2H_3^+$, $43C_2H_3O^+$) (Moffet and Prather, 2009). EC particles mainly originated from combustion processes (Bond et al., 2013). Strong $K^+$ ion signal observed here, it is likely that the aged EC particles in part are from biomass burning (Bi et al. 2011). The aged EC particle type was the largest fraction (49.3% by number) of the the total cloud residues (Figure S3). In addition, Nf of the aged EC residues significantly decreased from 54.1% in the size range of 0.2-1.0 μm to 19.2% in the size range of 1.1-1.9 μm (Figure 4). Note that the chemical composition of cloud residues is dependent on the particle size (Roth et al., 2016), and the number reported for each particle type might suffer the bias from size-dependent transmission efficiency (Qin et al., 2006). The relative fraction of cloud residues in 100 nm size interval is presented to minimize the influence of size-dependent transmission efficiency of single particle mass spectrometry (Roth et al., 2016).

The K-rich particles exhibited the highest peak at m/z $39K^+$, mainly combined with sulfate and nitrate (m/z $-46NO_2^-$, $-62NO_3^-$). The K-rich particles presumably result from biomass/biofuel burning source (Moffet et al., 2008; Pratt et al. 2011; Zhang et al., 2013).

Aged time 81-88 min of biomass burning particles show increase in the mass fractions of ammonium, sulfate, and nitrate (Pratt et al. 2011). In this study, the K-rich particles would be expected to experience aged process due to strong sulfate and nitrate signals (Hudson et al. 2004; Pratt et al. 2011). Aged biomass burning particles can participate in cloud droplets formation and show an effective CCN activity (Pratt et al. 2010a). The K-rich particle type, the second largest contributor, accounted for 33.9% by number of the the total cloud residues (Figure S3).

The abundant aged soot/EC and biomass burning particles were often detected in cloud residues (Pratt et al., 2010a; Roth et al., 2016). The contribution of local anthropogenic origins to aged soot and/or biomass burning particles in cloud/fog residues has been reported in Schmücke (Roth et al., 2016) and Guangzhou city (Bi et al., 2016). At the North Slope of Alaska, the measurement of biomass burning particles in cloud residues mainly resulted from Asia sources (Zelenyuk et al., 2010). Similarly, majority of aged EC and K-rich cloud residues observed here are expected to originate from long-range transportation due to insignificant sources of local anthropogenic emissions or fire dots. At the Jungfraujoch station (3,580 m a.s.l.) in Europe, the K-rich (biomass burning) particles was only found to contribute 3% of the cloud droplets and the aged EC cloud residue was insignificant (<1% by number) (Kamphus et al., 2010). The Jungfraujoch is a station where located mostly in the free troposphere and in a remote region, so the biomass burning contribution can be expected to be lower than at other sites.

The Amine particles were characterized by related amine ion signals at m/z 58$C_2H_5NHCH_2^+$ (diethylamine, DEA), 59$N(CH_3)_3^+$ (trimethylamine, TMA) and 86$C_5H_{12}N^+$ (triethylamine, TEA) (Angelino et al., 2001; Moffet et al., 2008; Pratt and

Prather, 2010). Note that amine peaks would be enhanced when using a 266 nm ionization laser and that the amines themselves may not comprise the majority of the particle mass (Pratt et al., 2009). This particle type also contained sulfuric acid ion signals at m/z -195H(HSO$_4$)$_2^-$, indicative of acidic particles (Rehbein et al., 2011). The Amine particles represented 3.8% by number of the total cloud residues (Figure S3). Higher Nf of the Amine residues was detected in size range from 0.7 to 1.9 μm relative to size range from 0.2 to 0.6 μm (16.7% versus 0.4%), as shown in Figure 4. Aqueous reaction improving the participation of amine has been observed in Guangzhou (Zhang et al., 2012a) and Southern Ontario (Rehbein et al., 2011). A recent study also shows a clear enhancement of amine-containing particles in cloud residues compared to the ambient particles (9% versus 2% by number) (Roth et al., 2016). It indicates a preferential formation of amine in cloud. However, this possibility was not supported by the observations of Bi et al. (2016), who did not detect amine-containing particles in fog residues. In this study, the Nf of the Amine particles varied from 0.2% to 15.1% of the total cloud residues dependent on air mass history (see Sect. 3.4).

The Dust particles presented significant ions at m/z 40Ca$^+$, 56CaO$^+$/Fe$^+$, 96Ca$_2$O$^+$ and -76SiO$_3^-$. Internal mixing with sulfate and nitrate in the Dust particle is expect to act as CCN (Twohy and Anderson 2008; Twohy et al., 2009; Matsuki et al., 2010), despite sulfate and nitrate partly contribution from in-cloud production. This type contributed 2.9% by number of the total cloud residues (Figure S3). A slightly increase in Nf of the Dust residues was observed in size range above 0.5 μm relative to below 0.5 μm (3.0% versus 1.0%). At Mt. Tai in northern China, a high concentration of Ca$^{2+}$ in cloud/fog water was mainly attributed to a sandstorm event during spring season (Wang et al., 2011). At Mt.

Heng in southern China, abundant crust-related elements (e.g., Al) observed in cloud water is due to Asian dust storms occurred on March-May (Li et al., 2017). Based on the backward trajectory, the site was less affected by sandstorm source in northwestern China during cloud events. Local dust emission by anthropogenic-disturbing soils or removing vegetation cover can be excluded as a result of forest protection. Additionally, dust residues may occupied larger CCN (Tang et al., 2016), which cannot be detected by the SPAMS. Therefore, a low fraction (2.9% by number) of dust cloud residue is reasonable in the present study.

The Fe particles had its typical ions at m/z $56Fe^+$ and internally mixed with sulfate and nitrate. The Fe particle type made up 4.1% by number of the total cloud residues. Approximately 16% of the Fe cloud residues contained $Ca^+$ peak (m/z 40). Relatively weak $Na^+$ and $K^+$ peaks in the Fe particles possibly contributes to anthropogenic sources (Zhang et al., 2014), especially northern air mass across iron/steel industrial activities in Yangtze River Mid-Reaches city clusters (Figure 2). These might suggest that the Fe residues was likely to have come from mixed sources. The presence of Fe in the cloud droplets play an important role in aqueous-phase $SO_2$ catalytic oxidation in cloud processing (Harris et al., 2013), thus accelerating the sulfate content of Fe-containing particles in cloud processing.

The Na-rich particles were mainly composed of ion peaks at m/z $23Na^+$ and $39K^+$ in the positive mass spectra, and nitrate and sulfate species in the negative mass spectra. The Na-rich particle type made up 3.0% by number of the total cloud residues. Na-rich particles were resulted from varied sources including industrial emissions, sea salt or dry lake beds (Moffet et al. 2008). The Nf of the Na-rich cloud residues did not increase from continental (Northerly) air mass to maritime (southwesterly) air mass on 21 Jan (3.3% versus 2.4% by number). However, related sea salt ion peak area (m/z, 81/83 $Na_2{}^{35}Cl/Na_2{}^{37}Cl$) were enhanced for Na-rich particles origination from maritime air mass relative to continental air mass (3.8 ± 2.4 times). Continental air masses crossed industrial areas where located in the Yangtze River Mid-Reaches city cluster (Figure 2). Industrial emissions was a possible contributor to Na-rich particles under the influence of continental air masses (Wang et al. 2016). This might suggests that the Na-rich particles were contributed from both the industrial emissions and sea salt. Therefore, under the influence of maritime air mass, the signals for sea salt contribution became obvious.

The OC, Pb and Other particle types contributed 0.1-2.3% by number to the total cloud residues (Figure S3). Their average mass spectra can be found in Figure S4. The OC particles presented dominant intense OC signals (e.g., m/z $27C_2H_3^+$, $37C_3H^+$, $43C_2H_3O^+$ and $51C_4H_3^+$) and abundant sulfate. Presence of $K^+$ signal was found in the OC particles suggesting possible biomass burning sources (Bi et al. 2011). The Pb particles showed its typical ions at m/z $208Pb^+$ and internally mixed with $K^+$ and $Cl^-$. Previous studies found that K and Cl internally mixed with Pb particles have a possible origination of waste incineration (Zhang et al., 2009) or iron and steel facility (Tsai et al., 2007). Internally mixed EC with metal signatures was observed in the Other particles.

Previous measurements found that dust, playa salts or sea salt particles are often enriched in larger cloud droplets (~20 μm) (Bator and Collett, 1997; Pratt et al., 2010b). Organic carbon tend to be enriched in small cloud/fog droplets, extending to 4 μm (Herckes et al., 2013). It is wealth to note that cloud droplets were above 8 μm in the present study. Thus, it partially leads to relatively larger fractions of the Dust and Na-rich cloud residues observed, and the less fractions of the OC cloud residues.

## 3.3 Mixing state of secondary species in cloud residues

The Nf of sulfate-containing particles were found to be highly related to the K-rich (91%), OC (100%), aged EC (98%), Pb (74%), Fe (93%) and Amine (99%) cloud residues, as shown in Figure 5. Lower Nf of sulfate-containing particles were observed in the Na-rich (41%) and Dust (42%) cloud residues. In contrast, nitrate-containing particles contributed 89% and 88% by number to the Na-rich and Dust cloud residues, respectively. The heterogeneous chemistry of $HNO_3$ in the Na-rich and Dust particles may lead to the preferential enrichment of nitrate (Li and Shao, 2009). Note that after activation, uptake of gas-phase $HNO_3$ would increase nitrate level in the cloud residues (Schneider et al., 2017). The detection of nitrate in the cloud residues was thought to be the form of ammonium-nitrate by estimating the ratio of m/z 30 to m/z 46 in AMS data (Drewnick et al., 2007; Hayden et al., 2008). Low portions of ammonium (m/z, $18NH_4^+$) in the Na-rich (23% by number) and Dust (15% by number) cloud residues suggest that in this region, ammonium nitrate was not a predominant form of nitrate in the two cloud residual type. The Na-rich and Dust types were mainly composed of alkaline ion peaks (m/z, $23Na^+$, $39K^+$ and $40Ca^+$) in the position mass spectra (Figure 3), accompanied with larger fraction (88-89%) of nitrate. It suggests that nitrate might exist in the form of $Ca(NO_3)_2$, $NaNO_3$ or $KNO_3$ in the Dust and Na-rich cloud residues. It should be noted that the evaporation chamber of the GCVI may lead to a reduction of ammonium nitrate in the cloud residues (Hayden et al., 2008). We found that nitrate-containing particles accounted for only 46% by number of the aged EC cloud residues, which is significantly less than the contribution of sulfate-containing particles. Previous studies found that aged EC (soot) fog/cloud residues are mainly internally mixed with sulfate (Pratt et al., 2010a; Harris et al., 2014; Bi et al., 2016). Aged EC particles mixed with sulfate are good CCN, rather than formed by in-cloud processing (Bi et al., 2016; Roth et al., 2016). High portions (75-86% by number) of ammonium-containing particles were observed for the OC and aged EC cloud residues, suggesting that ammonium will mostly be in the form of ammonium sulfate or ammonium nitrate for the two cloud residue types (Zhang et al., 2017). This result also implies that ammonium-containing particles are preferentially activated or enhanced by uptake of gaseous $NH_3$ to neutralize acidic cloud droplets for the OC and EC types.

Organics (e.g., amine and oxalate) have previously been measured in cloud water/residues (Sellegri et al., 2003; Sorooshian et al., 2007a; Pratt et al., 2010a). Amine and oxalate particles with mixtures of inorganic salts could enhance water uptake behavior (Sorooshian et al., 2008; Wu et al., 2011). The presence of TMA in the Amine cloud residues is expected to promote water uptake in sub- and supersaturated regimes (Sorooshian et al., 2007b). A total of 3,410 oxalate-containing particles (m/z, -89$HC_2O_4^-$) represented 14.4% by number of the total cloud residues, which was mainly associated with the K-rich cloud residues (~70% by number). Note that after activation, gas phase partitioning into condensed phase or in-cloud production pathways would increase oxalate level in cloud droplets (Sellegri et al., 2003; Pratt et al., 2010a). Relative high portions (~30% by number) of oxalate-containing particles in the metal (Pb, Fe) cloud residues might be the form of metal oxalate complexes from reactions of in-cloud formation oxalate with metals (Furukawa and Takahashi, 2011). Oxalate can readily partition into the particle phase to form amine salts (Pratt et al., 2009), it may facilitate the entrainment of oxalate (33% by number) in the Amine residues. A low fraction (4%) of oxalate-containing particles in the OC type is a result of restrictive classification. Classification of the OC particles mainly based on intense organic carbon ion signals (e.g., m/z 27$C_2H_3^+$, 37$C_3H^+$, 43$C_2H_3O^+$ and 51$C_4H_3^+$). However, majority of oxalate-containing particles internally mixed with the K-rich type. Therefore, oxalate was classified to the K-rich type, probably contributed from biomass burning. Noted that K-rich could contain a large abundant of organics (Pratt et al. 2011), however, the signals of organics were covered by the potassium due to its high sensitive to the laser.

### 3.4 Comparison of cloud residues in different air mass sources

Figure 6 displays hourly detected particle counts and Nf values of nine types of cloud residues and ambient particles. A very abrupt increase (decrease) in Nf of aged EC (Amine) particle types from cloud residues to ambient particles was observed on Jan 17. Ambient RH showed an abrupt decrease from nearly 100% at 10:00 to 85% at 11:00 on 17 Jan (Figure 1). Ambient temperature also decreased from 10 ℃ at 11:00 to 4 ℃ at 18:00 on 17 Jan (Figure 1). These changes imply that the air mass changed from southwesterly cloudy air to northerly cloud-free air around noon on 17 Jan (Figure 2). The entrained particles originated from northern air mass might have insufficient supersaturation to activate as cloud droplets. It is the reason that Nf of particle types abruptly varied from cloud residues to ambient particles on Jan 17 (Figure 6).

Ambient RH increased from 60% at 19:00 to nearly 100% at 21:00 on 18 Jan (Figure 1). Ambient temperature also increased from 1.3 ℃ at 22:00 on 18 Jan to 3.2 ℃ at 06:00 on 19 Jan (Figure 1). These changes imply that the air mass changed from northerly cloud-free air to southwesterly cloudy air at night on 18 Jan (Figure 2). During 18-19 Jan, the cloud residues and ambient particles showed similar chemical characteristics and were dominated by aged EC particles (Figure 6). A lack of significant variation in the Nf of particle types for this period suggests that nuclei particles originated from northerly cloud-free air could be activated to become cloud droplets. Note that ambient particles when a cloud-free event occurred at 11:00-17:00 on 19 Jan with a remaining high level of $PM_{2.5}$ (~ 22.7 μg $m^{-3}$). Southwesterly wind flow on 19-20 Jan was too weak (~ 2.75 m $s^{-1}$) to dilute particles originated from northerly air masses (Figure 1). Additionally, high RH (90%) air mass at height 1,500 m (a.s.l.) gradually moved to north China from 19 to 20 Jan (Figure S5). These might lead to similar residual particle types observed from 19 Jan to 20 Jan, although the site encountered southwesterly cloudy air on 19-20 Jan (Figure 2).

During 16-17 and 21-22 Jan, the cloud residues consisted of a high fraction of the Amine type, which significantly differed from the observation during 18-19 Jan. Clearly, the observations during 16-17 and 21-22 Jan were influenced by a strong southwesterly flow with a low value of $PM_{2.5}$ (~ 3 μg $m^{-3}$).

As mentioned above, the Nf of the cloud residue types significantly changed as the air mass origin varied from northerly to southwesterly. To further investigate the influence of air mass history, we selected cloud residues that had arrived from a northerly air mass on 18-19 Jan and compared these to cloud residues originating from a southwesterly air mass during the periods of 16-17 and 21-22 Jan. The detected number of cloud residues for the northerly and southwesterly air masses are given in Table S1. Note that southwesterly air mass accompanied by high relative humidity (90%) (Figure S5) may have triggered particles activated to CCN prior to their arrival to the sampling site.

The K-rich type was found to contribute 23.9% to the cloud residues in the northerly air mass, which was significantly lower than its contribution to the southwesterly air mass (51.5%), as shown in Figure 7. A similarity in averaged mass spectrum of the K-rich residues was found for the southwesterly and northerly air masses (Figure S6). The considerable increase of K-rich cloud residues suggests a major influence of regional biomass-burning activities. Biomass-burning emissions from Southeast Asia, including Myanmar, Vietnam, Laos and Thailand, where abundant fire dots are observed (Figure 2), could have been transported to the sampling site under a southwesterly air mass (Duncan et al., 2003). In contrast, the aged EC type represented only 23.7% of the cloud residues under the influence of the southwesterly air mass, which was significantly lower than observations for the northerly air mass (59.9%), as shown in Figure 7. This result suggests that the northern air mass has a greater influence on the presence of aged EC cloud residues.

In addition, an obvious increase in Nf of the Amine type was observed in the southwesterly air mass (15.1%) compared to the northerly air mass (0.2%), as shown in Figure 7. This implies that the sources or formation mechanisms of amine in cloud residues varied in different air masses. The southwesterly air mass arrived from as far as the Bay of Bengal and then travelled through Southeast Asia before reaching South China (Figure 2). The potential gas amine emissions from ocean (Facchini et al., 2008) and livestock areas (90 million animals, data was available at the website http://faostat3.fao.org) in Southeast Asia might promote the enrichment of amine particles. Note that after activation, the partitioning of the gas amine on cloud droplets may further contribute to the enhanced Amine cloud residues (Rehbein et al., 2011), especially for air masses delivered via routes with high relative humidity, as mentioned above (Figure S5). In contrast, northerly air mass accompanied with dry airstreams may inadequately induce the partitioning of gas amines into the particle phase (Rehbein et al., 2011).

### 3.5 Comparison of cloud residues with ambient and non-activated particles

A direct comparison between cloud residues and ambient particles was limited because of their differences in air mass origins. During the sampling period, the cloud events occurred once the southwesterly air masses were dominant. Therefore, a comparison between cloud residues and ambient particles cannot be addressed under the influence of southwesterly air masses. Here, we chose five hours before and after the beginning of the cloud II period in order to compare cloud residues and ambient particles with similar northerly air mass origins, as discussion in Sect. 3.4. The time and detected counts of cloud residues and ambient particles for this comparison are listed in Table S1.

From 10:00 21 Jan to 13:00 23 Jan, cloud residues and non-activated particles were alternately sampled with interval of one hour. Ambient temperature decreased from 6 ℃ at 11:00 to 0 ℃ at 23:00 on 22 Jan (Figure 1). Additionally, ambient particles level (residual and non-activated particles) showed a clearly increase from 121 $cm^{-3}$ to 1339 $cm^{-3}$ during this period (Figure S2). It suggests that initial mixing of northerly cloud-free air and southwesterly cloudy air around noon on 22 Jan. It is noted that non-activated particles were detected in size range above 200 nm, extending to 500 nm (Figure S7). The dry northern air mass might lower supersaturation, only larger particles could be activated. This might result in above 200 nm non-activated particles observed here (Mertes et al., 2005; Kleinman et al., 2012; Hammer et al., 2014). The detected particle counts in the cloud residues and non-activated particles are given in Table S1.

The contribution of K-rich particles in cloud residues slightly decreased relative to ambient particles (23.9% versus 30.7%), as shown in Figure 7. Previous studies also showed that no significant change in Nf of biomass-burning particles for cloud residues relative to ambient particles (Pratt et al., 2010a; Roth et al., 2016). The biomass-burning particles internally mixed with soluble species (e.g., sulfate, nitrate and oxalate) enhanced their ability to act as CCN, as discussion in Sect. 3.3. However, Kamphus et al. (2010) reported that biomass-burning particles account for only 3% of cloud residues compared with 43% of ambient particles, and they suspected that biomass-burning particles might exist in the form of tar balls (hydrophobic materials). A slight increase in Nf of the aged EC cloud residues was observed relative to ambient particles (59.9% versus 53.8%), as shown in Figure 7.  In general, freshly emitted EC particles are less hydrophilic and do not active as CCN (Bond et al., 2013). The aged EC particles show a high degree of internal mixing with secondary inorganic compounds in this study (Figure 5), improving their ability to act as CCN. The remaining particle types showed no clear differences in Nf between cloud residues and ambient particles.

In comparing the cloud residues with non-activated particles, a significant change in Nf was found for the aged EC and K-rich type. A higher Nf of K-rich particles and a lower Nf of EC particles were found for the cloud residues relative to the non-activated particles (Figure 7). Entrainment of northerly cloud-free air might lower supersaturation during this period. Aged EC particles may require very high supersaturation to grow into cloud droplets and thus, only form hydrated non-activated aerosol (Hallberg et al., 1994).

Figure 8 and 9 show differences in average mass spectra for cloud residues versus ambient particles, as well as cloud residues versus non-activated particles, respectively.

Nitrate intensity (average ion peak area) was found to enhance in the cloud residues compared to ambient particles. In addition, nitrate-containing particles has been observed to account for 70% of the cloud residues compared to 38% of the ambient particles. Drewnick et al. (2007) suggested that rather than sulfate, high nitrate content in pre-existing particles preferentially acted as cloud droplets. Compared with containing-nitrate ambient particles, larger size of containing-nitrate residues (Figure S8) is more likely to be uptake of gaseous $HNO_3$ during cloud process (Hayden et al. 2008; Roth et al., 2016). A recent study also confirmed that uptake of gaseous $HNO_3$ was an important contributor for increasing in nitrate level in the cloud residues (Schneider et al., 2017). Interestingly, we observed a decrease in nitrate intensity in cloud residues except dust type (Figure 9) and a large size distribution of nitrate-containing cloud residues (Figure S7) compared with non-activated particles. This result suggests that particle size, rather than nitrate content, plays a more important role in the activation of particles into cloud droplets.

Sulfate intensity was only observed to enhance for the OC cloud residues relative to both ambient and non-activated particles. Although the in-cloud addition of sulfate can be produced from aqueous Fe-catalyzed or oxidation by $H_2O_2/O_3$ reactions (Harris et al., 2014), sulfate intensity was found to diminish in the Fe cloud residues relative to ambient particles. Compared with non-activated particles, sulfate intensity was found to enhance in the Fe cloud residues. Additionally, sulfate-containing particles accounted for 94%, 93% and 94% of cloud residues, ambient and non-activated particles, respectively. Previous studies also showed that the mass or number fraction of sulfate-containing particles in the cloud residues changed between ambient and non-activated particles (Drewnick et al., 2007; Twohy and Anderson, 2008; Schneider et al., 2017). However, the reason for these changes remains unclear.

The in-cloud process has been reported to be an important pathway for the production of amine particles (Rehbein et al., 2011; Zhang et al., 2012a). In this study, no remarkable change in Nf of the Amine cloud residues was obtained relative to the ambient particles (0.2% versus 0.2%), as shown in Figure 7. Bi et al. (2016) considered that the absence of amine species in fog residues may be partially affected by droplet evaporation in the GCVI. We did find a high fraction of the Amine cloud residues when the southwesterly air mass prevailed, as discussion in Sect. 3.4. A lack of gas-phase amines may be the cause of few amine particles detected in the ambient particles and cloud residues (Rehbein et al., 2011). An increase in Nf of cloud residues was observed compared with non-activated particles (5.2% versus 0.1%), as shown in Figure 7. Increasing the particle water content facilitates partitioning of gas-phase amine species into the aqueous phase when gas-phase amines present (Rehbein et al., 2011).

## 4 Conclusions

This study presented an in situ observation of individual cloud residues, non-activated and ambient particles at a mountain site in South China. The finding shows that internal mixing with soluble species (e.g., sulfate) in EC particles was an important contributor to cloud residues in a remote area of China. Change in Nf of the cloud residue types influenced by various air masses highlights the important role of regional transportation in the observed cloud residual chemistry. Initial mixing of northerly cloud-free air and southwesterly cloudy air can induce the activation of the nuclei particles to become cloud droplets. Higher fractions of nitrate (88-89% by number) were found in the Dust and Na-rich cloud residues relative to sulfate (41-42%) and ammonium (15-23%). Higher fraction, intensity (average ion peak area) and larger size of nitrate-containing particles were found in the cloud residues relative to the ambient particles. This result is most likely the cause of the uptake from gas-phase $HNO_3$.

## Acknowledgments

This work was supported by the National Nature Science Foundation of China (No. 91544101 and 41405131), the National Key Research and Development Program of China (SQ2017ZY01014804) and the Foundation for Leading Talents of the Guangdong Province Government. The authors thank Ji Ou from Shaoguan city Environmental Monitoring Center for the support at the observed site. We also acknowledge the NOAA Air Resources Laboratory (ARL) for the provision of the HYSPLIT transport and dispersion model and/or READY website (http://ready.arl.noaa.gov) used in this publication. All the data can be obtained by contacting the corresponding author.

## References

Andreae, M. O. and Rosenfeld, D.: Aerosol-cloud-precipitation interactions. Part 1. The nature and sources of cloud-active aerosols, Earth-Sci. Revi., 89, 13-41, doi: 10.1016/j.earscirev.2008.03.001, 2008.

Angelino, S., Suess, D.T. and Prather, K. A.: Formation of aerosol particles from reactions of secondary and tertiary alkylamines: Characterization by aerosol time-of-flight mass spectrometry, Environ. Sci. Technol., 35, 3130-3138, doi: 10.1021/es0015444, 2001.

Bator, A. and Collett, J.L.: Cloud chemistry varies with drop size, J. Geophys. Res. Atmos., 102, 28071-28078. 1997.

Bi, X., Lin, Q., Peng, L., Zhang, G., Wang, X., Brechtel, F. J., Chen, D., Li, M., Peng, P. a., Sheng, G. and Zhou, Z.: In situ detection of the chemistry of individual fog droplet residues in the Pearl River Delta region, China, J. Geophys. Res. Atmos., 121(15), 9105-9116, doi:10.1002/2016jd024886, 2016.

Bi, X., Zhang, G., Li, L., Wang, X., Li, M., Sheng, G., Fu, J. and Zhou, Z.: Mixing state of biomass burning particles by single particle aerosol mass spectrometer in the urban area of PRD, China. Atmos. Environ., 45, 3447-3453, doi:10.1016/j.atmosenv.2011.03.034, 2011.

Berg, L.K., Berkowitz, C.M., Hubbe, J.M., Ogren, J.A., Hostetler, C.A., Ferrare, R.A., Hair, J.W., Dubey, M.K., Mazzoleni, C. and Andrews, E.: Overview of the cumulus humilis aerosol processing study, B. Am. Meteorol. Soc. 90, 1653-1667, http://dx.doi.org/10.1175/2009BAMS2760.1, 2009.

Bond, T. C., Doherty, S. J., Fahey, D. W., Forster, P. M., Berntsen, T., DeAngelo, B. J., Flanner, M. G., Ghan, S., Kärcher, B., Koch, D., Kinne, S., Kondo, Y., Quinn, P. K., Sarofim, M. C., Schultz, M. G., Schulz, M., Venkataraman, C., Zhang, H., Zhang, S., Bellouin, N., Guttikunda, S. K., Hopke, P. K., Jacobson, M. Z., Kaiser, J. W., Klimont, Z., Lohmann, U., Schwarz, J. P., Shindell, D., Storelvmo, T., Warren, S. G. and Zender, C. S.: Bounding the role of black carbon in the climate system: A scientific assessment, J. Geophys. Res. Atmos., 118, 5380-5552, doi:10.1002/jgrd.50171, 2013.

Boucher, O., Randall, D., Artaxo, P., Bretherton, C., Feingold, G., Forster, P., Kerminen, V., Kondo,Y., Liao, H., Lohmann, U., Rasch, P., Satheesh, S., Sherwood, S., Stevens, B.

and Zhang X.: Clouds and Aerosols. In Climate Change 2013: The Physical Science Basis. Contribution of Working Group I to the Fifth Assessment Report of the Intergovernmental Panel on Climate Change [Stocker, T.F., D. Qin, G.-K. Plattner, M. Tignor, S.K. Allen, J. Boschung, A. Nauels, Y. Xia, V. Bex and P.M. Midgley (eds.)]. Cambridge University Press, Cambridge, United Kingdom and New York, NY, USA. 2013

Coggon, M.M., Sorooshian, A., Wang, Z., Craven, J.S., Metcalf, A.R., Lin, J.J., Nenes, A., Jonsson, H.H., Flagan, R.C. and Seinfeld, J.H.: Observations of continental biogenic impacts on marine aerosol and clouds off the coast of California, J. Geophys. Res. Atmos., 119, 6724-6748. doi:10.1002/2013JD021228, 2014.

Cziczo, D.J., Murphy, D.M., Hudson, P.K. and Thomson, D.S.: Single particle measurements of the chemical composition of cirrus ice residue during CRYSTAL-FACE, J. Geophys. Res. Atmos., 109, D04201, doi:10.1029/2003JD004032, 2004.

Cziczo, D.J., Froyd, K.D., Hoose, C., Jensen, E.J., Diao, M., Zondlo, M.A., Smith, J.B., Twohy, C.H. and Murphy, D.M.: Clarifying the dominant sources and mechanisms of cirrus cloud formation, Science, 340, 1320-1324. doi: 10.1126/science.1234145,2013.

Drewnick, F., Schneider, J., Hings, S. S., Hock, N., Noone, K., Targino, A., Weimer, S. and Borrmann, S.: Measurement of ambient, interstitial, and residual aerosol particles on a mountaintop site in central Sweden using an aerosol mass spectrometer and a CVI, J. Atmos. Chem., 56, 1-20, doi:10.1007/s10874-006-9036-8, 2007.

Deng, X., Wu, D., Shi, Y., Tang, H., Fan, S., Huang, H., Mao, W. and Ye, Y.: Comprehensive analysis of the macro-and micro-physical characteristics of dense fog in the area south of the Nanling Mountains (in Chinese), J.Trop. Meteorol., 23, 424-434. 2007.

Duncan, B. N., Martin, R. V., Staudt, A. C., Yevich, R. and Logan, J. A.: Interannual and seasonal variability of biomass burning emissions constrained by satellite observations, J. Geophys. Res. Atmos., 108(D2), doi:108, 10.1029/2002jd002378, 2003.

Freud, E., Rosenfeld, D., Andreae, M.O., Costa, A.A. and Artaxo, P.: Robust relations between CCN and the vertical evolution of cloud drop size distribution in deep convective clouds, Atmos. Chem. Phys., 8, 1661-1675, 2008.

Facchini, M. C., Decesari, S., Rinaldi, M., Carbone, C., Finessi, E., Mircea, M., Fuzzi, S., Moretti, F., Tagliavini, E. and Ceburnis, D.: Important source of marine secondary organic aerosol from biogenic amines, Environ. Sci. Technol., 42, 9116-9121, doi: 10.1021/es8018385, 2008.

Furukawa, T. and Takahashi, Y.: Oxalate metal complexes in aerosol particles: implications for the hygroscopicity of oxalate-containing particles, Atmos. Chem. Phys., 11, 4289-4301, doi:10.5194/acp-11-4289-2011, 2011.

Hallberg, A., Ogren, J. A., Noone, K. J., Okada, K., Heintzenberg, J. and Svenningsson, I. B.: The influence of aerosol particle composition on cloud droplet formation, J. Atmos. Chem., 19, 153-171, doi: 10.1007/978-94-011-0313-8_8,1994.

Harris, E., Sinha, B., van Pinxteren, D., Tilgner, A., Fomba, K. W., Schneider, J., Roth, A., Gnauk, T., Fahlbusch, B. and Mertes, S.: Enhanced role of transition metal ion catalysis during in-cloud oxidation of $SO_2$, Science, 340, 727-730, doi:10.1126/science.1230911, 2013.

Harris, E., Sinha, B., van Pinxteren, D., Schneider, J., Poulain, L., Collett, J., D'Anna, B., Fahlbusch, B., Foley, S., Fomba, K. W., George, C., Gnauk, T., Henning, S., Lee, T., Mertes, S., Roth, A., Stratmann, F., Borrmann, S., Hoppe, P. and Herrmann, H.: In-cloud sulfate addition to single particles resolved with sulfur isotope analysis during HCCT-2010, Atmos. Chem. Phys., 14, 4219-4235, doi:10.5194/acp-14-4219-2014, 2014.

Hammer, E., Gysel, M., Roberts, G.C., Elias, T., Hofer, J., Hoyle, C.R., Bukowiecki, N., Dupont, J.C., Burnet, F., Baltensperger, U. and Weingartner, E.: Size-dependent particle activation properties in fog during the ParisFog 2012/13 field campaign, Atmos. Chem. Phys., 14, 10517-10533, 2014.

Hayden, K. L., Macdonald, A. M., Gong, W., Toom-Sauntry, D., Anlauf, K. G., Leithead, A., Li, S. M., Leaitch, W. R. and Noone, K.: Cloud processing of nitrate, J. Geophys. Res. Atmos., 113(D18), doi:10.1029/2007jd009732, 2008.

Herich, H., Kammermann, L., Gysel, M., Weingartner, E., Baltensperger, U., Lohmann, U. and Cziczo, D. J.: In situ determination of atmospheric aerosol composition as a function of hygroscopic growth, J. Geophys. Res. Atmos., 113(D16), doi:10.1029/2008jd009954, 2008.

Herckes, P., Valsaraj, K.T. and Collett, J.L., A review of observations of organic matter in fogs and clouds: Origin, processing and fate, Atmos. Res., 132, 434-449. 2013.

Hudson, P.K., Murphy, D.M., Cziczo, D.J., Thomson, D.S., de Gouw, J.A., Warneke, C., Holloway, J., Jost, H.J. and Hübler, G.: Biomass-burning particle measurements: Characteristic composition and chemical processing, J. Geophys. Res. Atmos., 109, D23S27, doi:10.1029/2003JD004398, 2004.

Kamphus, M., Ettner-Mahl, M., Klimach, T., Drewnick, F., Keller, L., Cziczo, D. J., Mertes, S., Borrmann, S. and Curtius, J.: Chemical composition of ambient aerosol, ice residues and cloud droplet residues in mixed-phase clouds: single particle analysis during the Cloud and Aerosol Characterization Experiment (CLACE 6), Atmos. Chem. Phys., 10, 8077-8095, doi:10.5194/acp-10-8077-2010, 2010.

Kleinman, L.I., Daum, P.H., Lee, Y.-N., Lewis, E.R., Sedlacek III, A., Senum, G., Springston, S., Wang, J., Hubbe, J. and Jayne, J.: Aerosol concentration and size distribution measured below, in, and above cloud from the DOE G-1 during VOCALS-Rex, Atmos. Chem. Phys., 12, 207-223, 2012.

Lee, C. S. L., Li, X., Zhang, G., Peng, X. and Zhang, L.: Biomonitoring of trace metals in the atmosphere using moss (Hypnum plumaeforme) in the Nanling Mountains and the Pearl River Delta, Southern China. Atmos. Environ., 39(3), 397-407, 2005.

Li, L., Huang, Z., Dong, J., Li, M., Gao, W., Nian, H., Fu, Z., Zhang, G., Bi, X. and Cheng, P.: Real time bipolar time-of-flight mass spectrometer for analyzing single aerosol particles, Int. J. Mass Spectrom., 303, 118-124, doi:http://dx.doi.org/10.1016/j.ijms.2011.01.017, 2011a.

Li, T., Wang, Y., Zhou, J., Wang, T., Ding, A., Nie, W., Xue, L., Wang, X. and Wang, W.: Evolution of trace elements in the planetary boundary layer in southern China: effects of dust storms and aerosol-cloud interaction, J. Geophys. Res. Atmos., 122, 3492-3506, 2017.

Li, W., Li, P., Sun, G., Zhou, S., Yuan, Q. and Wang, W.: Cloud residues and interstitial aerosols from non-precipitating clouds over an industrial and urban area in northern China, Atmos. Environ., 45, 2488-2495, doi:10.1016/j.atmosenv.2011.02.044, 2011b.

Lohmann, U., Stier, P., Hoose, C., Ferrachat, S., Kloster, S., Roeckner, E. and Zhang, J.: Cloud microphysics and aerosol indirect effects in the global climate model ECHAM5-HAM, Atmos. Chem. Phys., 7, 3425-3446, 2007.

Matsuki, A., Schwarzenboeck, A., Venzac, H., Laj, P., Crumeyrolle, S. and Gomes, L.: Cloud processing of mineral dust: direct comparison of cloud residual and clear sky particles during AMMA aircraft campaign in summer 2006, Atmos. Chem. Phys., 10, 1057-1069, 2010.

McFiggans, G., Artaxo, P., Baltensperger, U., Coe, H., Facchini, M. C., Feingold, G., Fuzzi, S., Gysel, M., Laaksonen, A. and Lohmann, U.: The effect of physical and chemical aerosol properties on warm cloud droplet activation, Atmos. Chem. Phys., 6, 2593-2649, doi:10.5194/acp-6-2593-2006, 2006.

Mertes, S., Lehmann, K., Nowak, A., Massling, A. and Wiedensohler, A.: Link between aerosol hygroscopic growth and dropletactivation observed for hill-capped clouds at connected flow conditions during FEBUKO, Atmos. Environ., 39, 4247-4256, 2005.

Moffet, R.C., Foy, B. D., Molina, L. A., Molina, M. and Prather, K.A.: Measurement of ambient aerosols in northern Mexico City by single particle mass spectrometry, Atmos. Chem. Phys., 8, 4499-4516, doi:10.5194/acp-8-4499-2008, 2008.

Moffet, R.C. and Prather, K.A.: In-situ measurements of the mixing state and optical properties of soot with implications for radiative forcing estimates, Proc. Natl. Acad. Sci. USA, 106, 11872-11877, doi: 10.1073/pnas.0900040106, 2009.

Pratt, K.A., Hatch, L. E. and Prather, K. A.: Seasonal volatility dependence of ambient particle phase amines, Environ. Sci. Technol., 43, 5276-5281, doi:10.1021/es803189n, 2009.

Pratt, K.A., Heymsfield, A. J., Twohy, C. H., Murphy, S. M., DeMott, P. J., Hudson, J. G., Subramanian, R., Wang, Z., Seinfeld, J. H. and Prather, K. A.: In Situ Chemical Characterization of Aged Biomass-Burning Aerosols Impacting Cold Wave Clouds, J. Atmos. Sci., 67, 2451-2468, doi:10.1175/2010jas3330.1, 2010a.

Pratt, K.A., Murphy, S., Subramanian, R., DeMott, P., Kok, G., Campos, T., Rogers, D., Prenni, A., Heymsfield, A. and Seinfeld, J.: Flight-based chemical characterization of biomass burning aerosols within two prescribed burn smoke plumes, Atmos. Chem. Phys., 11, 12549-12565, doi:10.5194/acp-11-12549-2011, 2011.

Pratt, K.A., Twohy, C.H., Murphy, S.M., Moffet, R.C., Heymsfield, A.J., Gaston, C.J., DeMott, P.J., Field, P.R., Henn, T.R., Rogers, D.C., Gilles, M.K., Seinfeld, J.H. and Prather, K.A.: Observation of playa salts as nuclei in orographic wave clouds, J. Geophys. Res. Atmos., 115, D15301, doi:10.1029/2009JD013606, 2010b.

Qin, X., Bhave, P.V. and Prather, K. A.: Comparison of two methods for obtaining quantitative mass concentrations from aerosol time-of-flight mass spectrometry measurements, Anal. Chem., 78(17), 6169-6178, doi: 10.1021/ac060395q, 2006.

Rehbein, P. J., Jeong, C. H., McGuire, M. L., Yao, X., Corbin, J. C. and Evans, G. J.: Cloud and fog processing enhanced gas-to-particle partitioning of trimethylamine, Environ. Sci. Technol., 45, 4346-4352, doi:10.1021/es1042113, 2011.

Rosenfeld, D., Lohmann, U., Raga, G.B., O'Dowd, C.D., Kulmala, M., Fuzzi, S., Reissell, A. and Andreae, M.O.: Flood or drought: how do aerosols affect precipitation?, Science, 321, 1309-1313, doi: 10.1126/science.1160606, 2008.

Roth, A., Schneider, J., Klimach, T., Mertes, S., van Pinxteren, D., Herrmann, H. and Borrmann, S.: Aerosol properties, source identification, and cloud processing in orographic clouds measured by single particle mass spectrometry on a central European mountain site during HCCT-2010, Atmos. Chem. Phys., 16, 505-524, doi:10.5194/acp-16-505-2016, 2016.

Schneider, J., Mertes, S., van Pinxteren, D., Herrmann, H. and Borrmann, S.: Uptake of nitric acid, ammonia, and organics in orographic clouds: Mass spectrometric analyses of droplet residual and interstitial aerosol particles, Atmos. Chem. Phys., 17, 1571-1593, doi:10.5194/acp-17-1571-2017, 2017.

Seinfeld, J.H., Bretherton, C., Carslaw, K.S., Coe, H., DeMott, P.J., Dunlea, E.J., Feingold, G., Ghan, S., Guenther, A.B. and Kahn, R.: Improving our fundamental understanding of the role of aerosol-cloud interactions in the climate system, Proc. Natl. Acad. Sci. USA, 113, 5781-5790, doi: 10.1073/pnas.1514043113, 2016.

Sellegri, K., Laj, P., Marinoni, A., Dupuy, R., Legrand, M. and Preunkert, S.: Contribution of gaseous and particulate species to droplet solute composition at the Puy de Dôme, France, Atmos. Chem. Phys., 3, 1509-1522, doi:10.5194/acp-3-1509-2003, 2003.

Shingler, T., Dey, S., Sorooshian, A., Brechtel, F. J., Wang, Z., Metcalf, A., Coggon, M., Mülmenstädt, J., Russell, L. M., Jonsson, H. H. and Seinfeld, J. H.: Characterisation and airborne deployment of a new counterflow virtual impactor inlet, Atmos. Meas. Tech., 5, 1259-1269, doi:10.5194/amt-5-1259-2012, 2012.

Song, X.H., Hopke, P. K., Fergenson, D. P. and Prather, K. A.: Classification of single particles analyzed by ATOFMS using an artificial neural network, ART-2A, Anal. Chem., 71, 860-865, doi:10.1021/ac9809682, 1999.

Sorooshian, A., Ng, N. L., Chan, A. W. H., Feingold, G., Flagan, R. C. and Seinfeld, J. H.: Particulate organic acids and overall water-soluble aerosol composition measurements from the 2006 Gulf of Mexico Atmospheric Composition and Climate Study (GoMACCS), J. Geophys. Res. Atmos., 112(D13), doi:10.1029/2007JD008537, 2007a.

Sorooshian, A., Lu, M. L., Brechtel, F. J., Jonsson, H., Feingold, G., Flagan, R. C. and Seinfeld, J. H.: On the source of organic acid aerosol layers above clouds, Environ. Sci. Technol., 41, 4647-4654, doi: 10.1021/es0630442, 2007b.

Sorooshian, A., Murphy, S., Hersey, S., Gates, H., Padro, L., Nenes, A., Brechtel, F., Jonsson, H., Flagan, R. and Seinfeld, J.: Comprehensive airborne characterization of aerosol from a major bovine source, Atmos. Chem. Phys., 8, 5489-5520, doi: http://dx.doi.org/10.5194/acp-8-5489-2008, 2008.

Stier, P., Feichter, J., Kinne, S., Kloster, S., Vignati, E., Wilson, J., Ganzeveld, L., Tegen, I., Werner, M. and Balkanski, Y.: The aerosol-climate model ECHAM5-HAM, Atmos. Chem. Phys., 5, 1125-1156. 2005.

Tang, M., Cziczo, D. J. and Grassian, V. H.: Interactions of Water with Mineral Dust Aerosol: Water Adsorption, Hygroscopicity, Cloud Condensation, and Ice Nucleation, Chem. Rev., doi:10.1021/acs.chemrev.5b00529, 2016.

Targino, A.C., Krejci, R., Noone, K.J. and Glantz, P.: Single particle analysis of ice crystal residuals observed in orographic wave clouds over Scandinavia during INTACC experiment, Atmos. Chem. Phys., 6, 1977-1990, 2006.

Tsai, J.H., Lin, K.H., Chen, C.Y., Ding, J.Y., Choa, C.G. and Chiang, H.L.: Chemical constituents in particulate emissions from an integrated iron and steel facility, J. Hazard. Mater., 147, 111-119. 2007.

Twohy, C.H., Kreidenweis, S.M., Eidhammer, T., Browell, E.V., Heymsfield, A.J., Bansemer, A.R., Anderson, B.E., Chen, G., Ismail, S., DeMott, P.J. and Van Den Heever, S.C.: Saharan dust particles nucleate droplets in eastern Atlantic clouds, Geophys. Res. Lett., 36, doi: 10.1029/2008GL035846, 2009.

Twohy, C.H. and Poellot, M.: Chemical characteristics of ice residual nuclei in anvil cirrus clouds: evidence for homogeneous and heterogeneous ice formation, Atmos. Chem. Phys., 5, 2289-2297, 2005.

Twohy C.H. and Anderson J. R.: Droplet nuclei in non-precipitating clouds: composition and size matter. Environ. Res. Lett., 3, 045002, doi:10.1088/1748-9326/3/4/045002, 2008.

Wang, H., An, J., Shen, L., Zhu, B., Xia, L., Duan, Q. and Zou, J.: Mixing state of ambient aerosols in Nanjing city by single particle mass spectrometry, Atmos. Environ., 132, 123-132, 2016.

Wang, Y., Guo, J., Wang, T., Ding, A., Gao, J., Zhou, Y., Collett, J. L. and Wang, W.: Influence of regional pollution and sandstorms on the chemical composition of cloud/fog at the summit of Mt. Taishan in northern China, Atmos. Res., 99, 434-442, doi:10.1016/j.atmosres.2010.11.010, 2011.

Wu, Z., Nowak, A., Poulain, L., Herrmann, H., and Wiedensohler, A.: Hygroscopic behavior of atmospherically relevant water-soluble carboxylic salts and their influence on the water uptake of ammonium sulfate, Atmos. Chem. Phys., 11, 12617-12626, doi:10.5194/acp-11-12617-2011, 2011.

Zelenyuk, A., Imre, D., Earle, M., Easter, R., Korolev, A., Leaitch, R., Liu, P., Macdonald, A. M., Ovchinnikov, M. and Strapp, W.: In Situ Characterization of Cloud Condensation Nuclei, Interstitial, and Background Particles Using the Single Particle Mass Spectrometer, SPLAT II†, Anal. Chem., 82, 7943-7951, doi:10.1021/ac1013892, 2010.

Zhang, Khalizov, A. F., Pagels, J., Zhang, D., Xue, H. and McMurry, P. H.: Variability in morphology, hygroscopicity, and optical properties of soot aerosols during atmospheric processing, Proc. Natl. Acad. Sci. USA, 105, 10291-10296, doi:10.1073/pnas.0804860105, 2008.

Zhang, G., Bi, X., Chan, L. Y., Li, L., Wang, X., Feng, J., Sheng, G., Fu, J., Li, M. and Zhou, Z.: Enhanced trimethylamine-containing particles during fog events detected by single particle aerosol mass spectrometry in urban Guangzhou, China, Atmos. Environ., 55, 121-126, doi:10.1016/j.atmosenv.2012.03.038, 2012a.

Zhang, G., Bi, X., Li, L., Chan, L. Y., Li, M., Wang, X., Sheng, G., Fu, J. and Zhou, Z.: Mixing state of individual submicron carbon-containing particles during spring and fall seasons in urban Guangzhou, China: a case study, Atmos. Chem. Phys., 13, 4723-4735, doi:10.5194/acp-13-4723-2013, 2013.

Zhang, G., Bi, X., Lou, S., Li, L., Wang, H., Wang, X., Zhou, Z., Sheng, G., Fu, J. and Chen, C.: Source and mixing state of iron-containing particles in Shanghai by individual particle analysis, Chemosphere, 95, 9-16, 2014.

Zhang, G., Lin, Q., Peng, L., Bi, X., Lei, M., Chen, D., Brechtel, F.J., Chen, X., Yan, W.,Wang, X., Peng, P., Sheng., G. and Zhou, Z.: Single particle mixing state and cloud scavenging of black carbon at a high-altitude mountain site in south China, J. Geophys. Res. Atmos. in revise, 2017.

Zhang, X., Wang, Y., Niu, T., Zhang, X., Gong, S., Zhang, Y. and Sun, J.: Atmospheric aerosol compositions in China: spatial/temporal variability, chemical signature, regional haze distribution and comparisons with global aerosols, Atmos. Chem. Phys., 12, 779-799, doi:10.5194/acp-12-779-2012, 2012b.

Zhang, Y.P., Wang, X.F., Chen, H., Yang, X., Chen, J.M. and Allen, J.O.: Source apportionment of lead-containing aerosol particles in Shanghai using single particle mass spectrometry, Chemosphere, 74, 501-507, 2009.

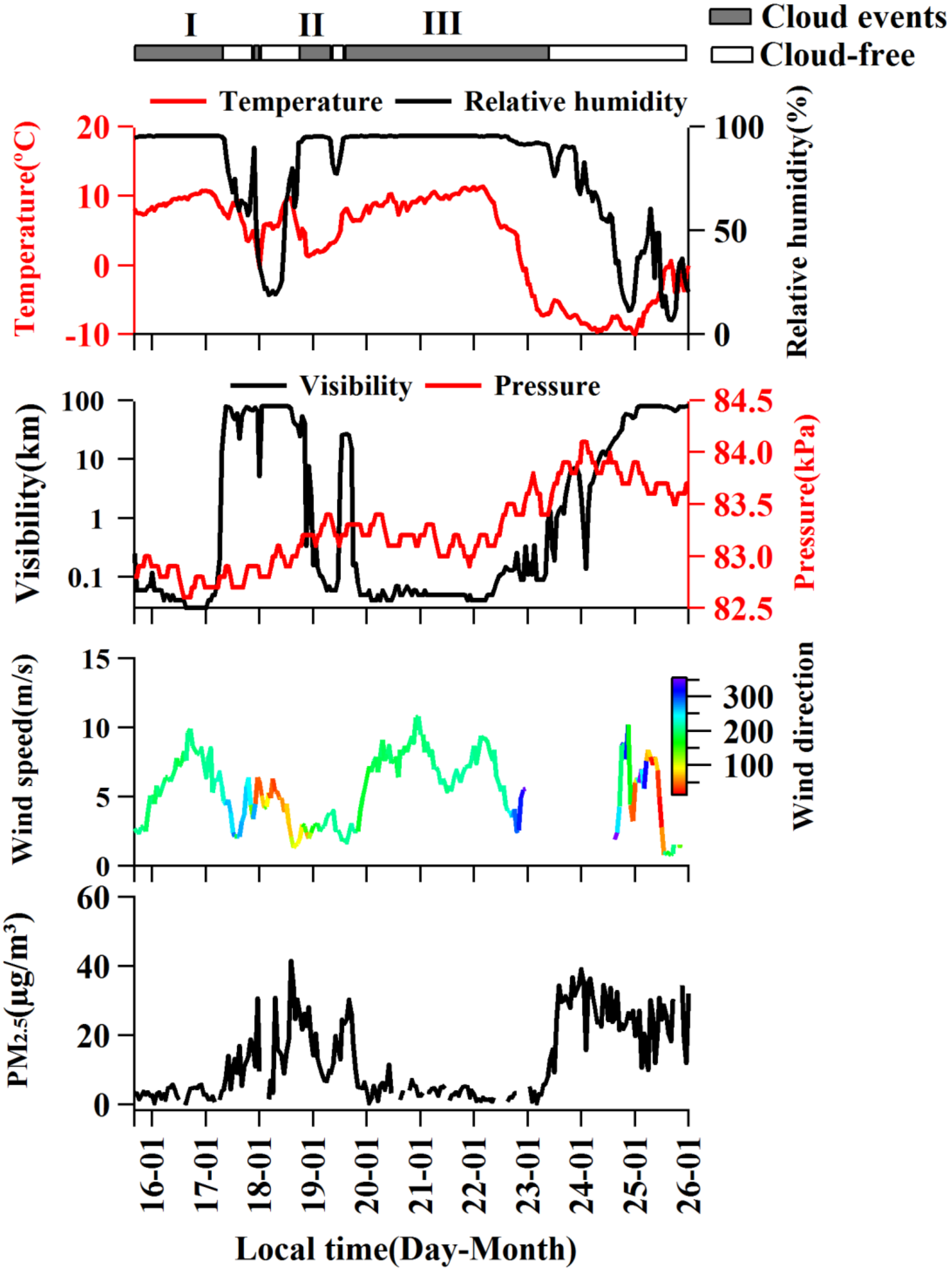

Figure 1: The hourly average variations in meteorological conditions (temperature, relative humidity, visibility, pressure, wind speed and direction) and $PM_{2.5}$.

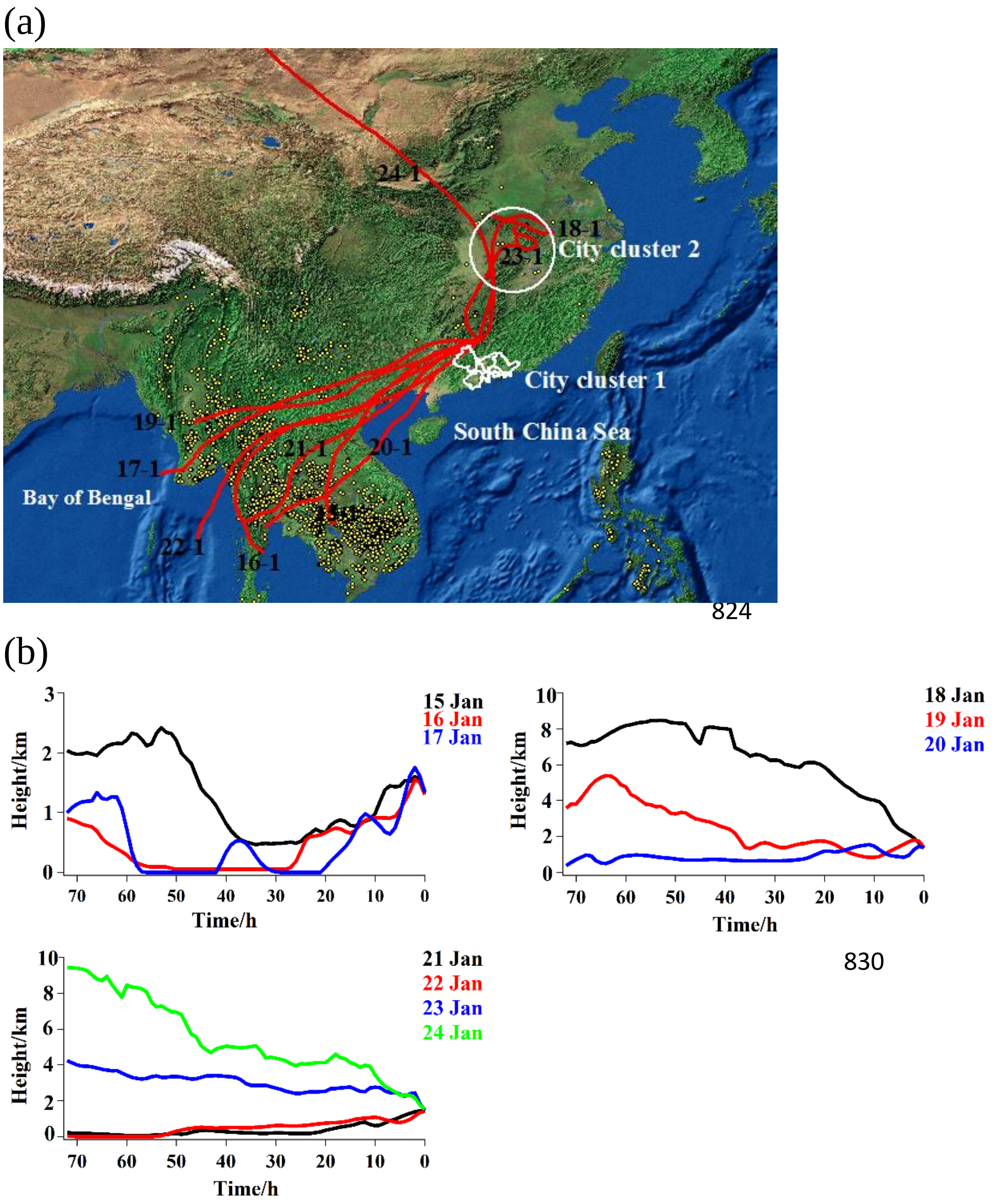

Figure 2: (a) HYSPLIT back trajectories (72 h) for air masses at 1,800 m during the whole sampling period. The white borders and circle refer to the Pearl River Delta (city cluster 1) and Yangtze River Mid-Reaches city clusters (city cluster 2), respectively. The yellow rots represent fire dots during the study periods. The fire dots are available at

https://earthdata.nasa.gov/; (b) Heights (above model ground) of the air masses as a function of time.

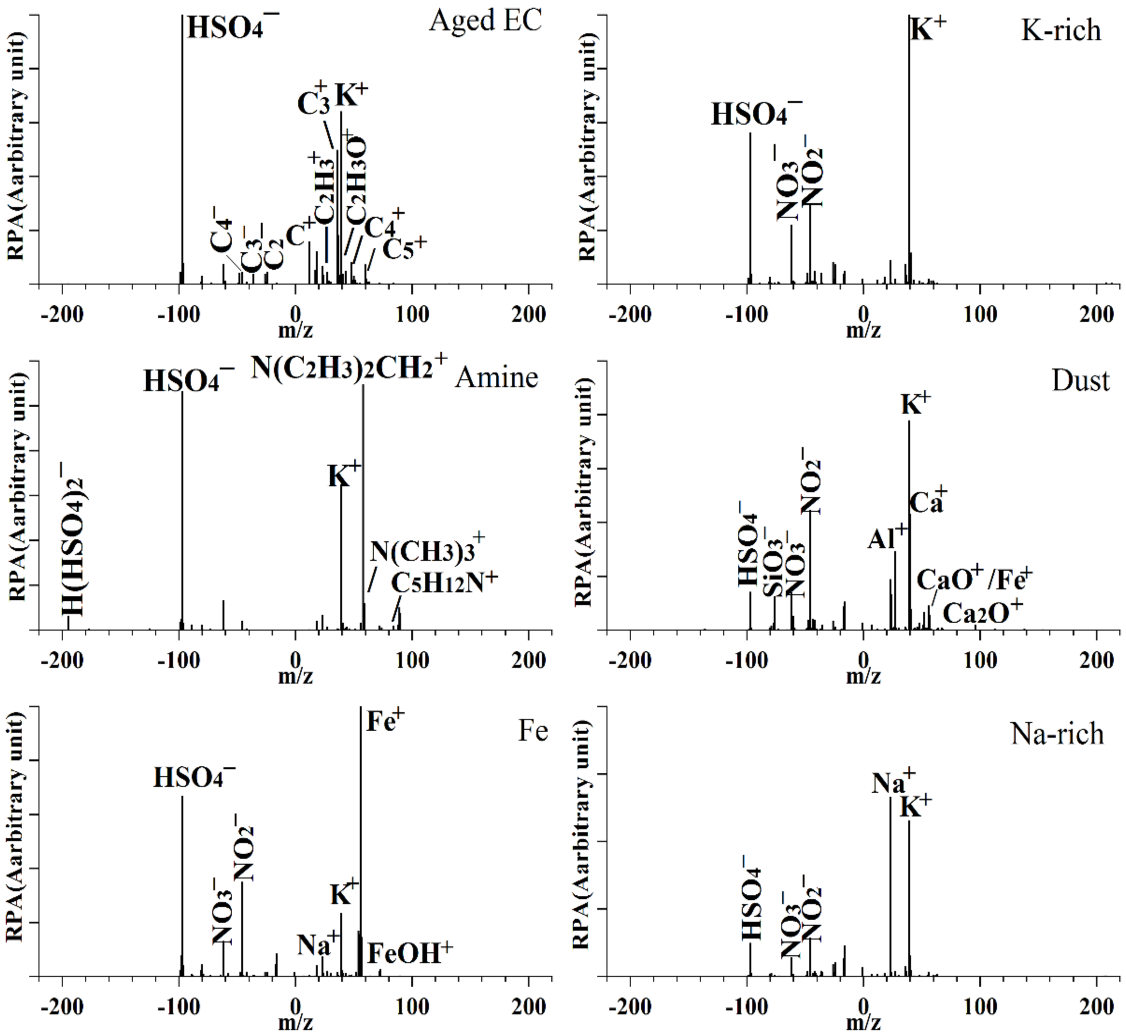

Figure 3: Averaged positive and negative mass spectra for the main 6 particle types (Aged EC, K-rich, Amine, Dust, Fe, Na-rich) of the sampled particles during the whole sampling period. RPA in the vertical axis refers to relative peak area. m/z in the horizontal axis represents mass-to-charge ratio.

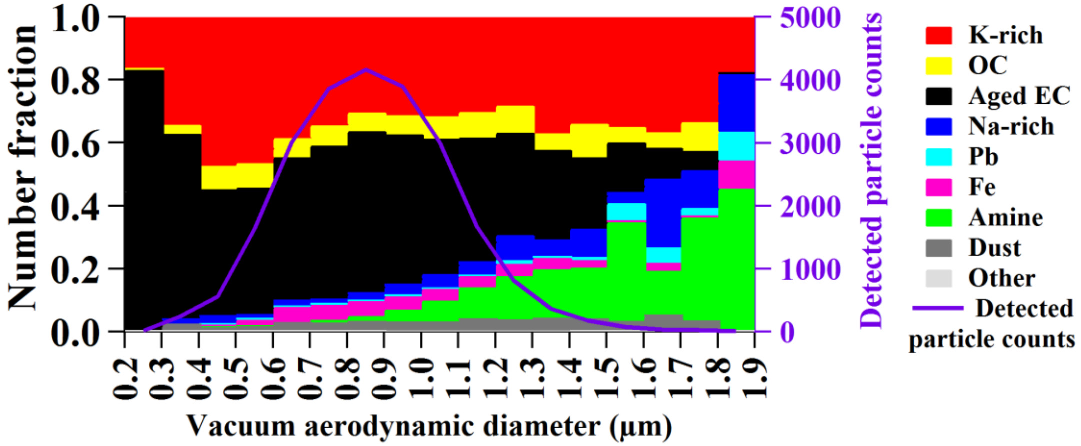

Figure 4: Number fraction for size distribution of the cloud residual types in 100 nm size intervals.

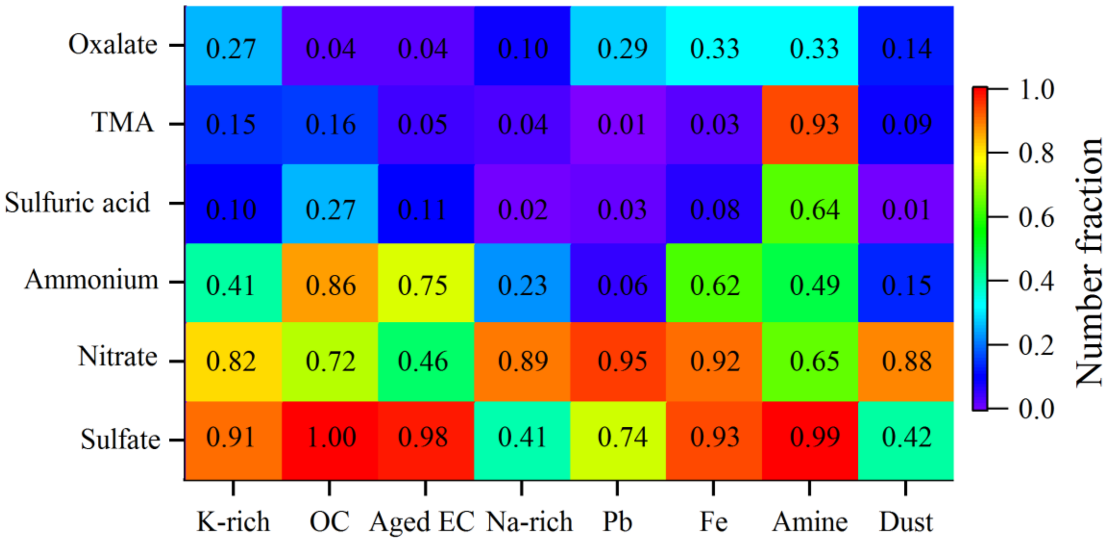

|  | K-rich | OC | Aged EC | Na-rich | Pb | Fe | Amine | Dust |
|---|---|---|---|---|---|---|---|---|
| Oxalate | 0.27 | 0.04 | 0.04 | 0.10 | 0.29 | 0.33 | 0.33 | 0.14 |
| TMA | 0.15 | 0.16 | 0.05 | 0.04 | 0.01 | 0.03 | 0.93 | 0.09 |
| Sulfuric acid | 0.10 | 0.27 | 0.11 | 0.02 | 0.03 | 0.08 | 0.64 | 0.01 |
| Ammonium | 0.41 | 0.86 | 0.75 | 0.23 | 0.06 | 0.62 | 0.49 | 0.15 |
| Nitrate | 0.82 | 0.72 | 0.46 | 0.89 | 0.95 | 0.92 | 0.65 | 0.88 |
| Sulfate | 0.91 | 1.00 | 0.98 | 0.41 | 0.74 | 0.93 | 0.99 | 0.42 |

Figure 5: Mixing state of secondary markers with the total cloud residues types; Sulfate (m/z, -97$HSO_4^-$), Nitrate (m/z, -46$NO_2^-$ or -62$NO_3^-$), Ammonium (m/z, 18$NH_4^+$), Sulfuric acid (m/z, -195$H(HSO_4)_2^-$), TMA (m/z, 59$N(CH_3)_3^+$), Oxalate (m/z, -89$HC_2O_4^-$).

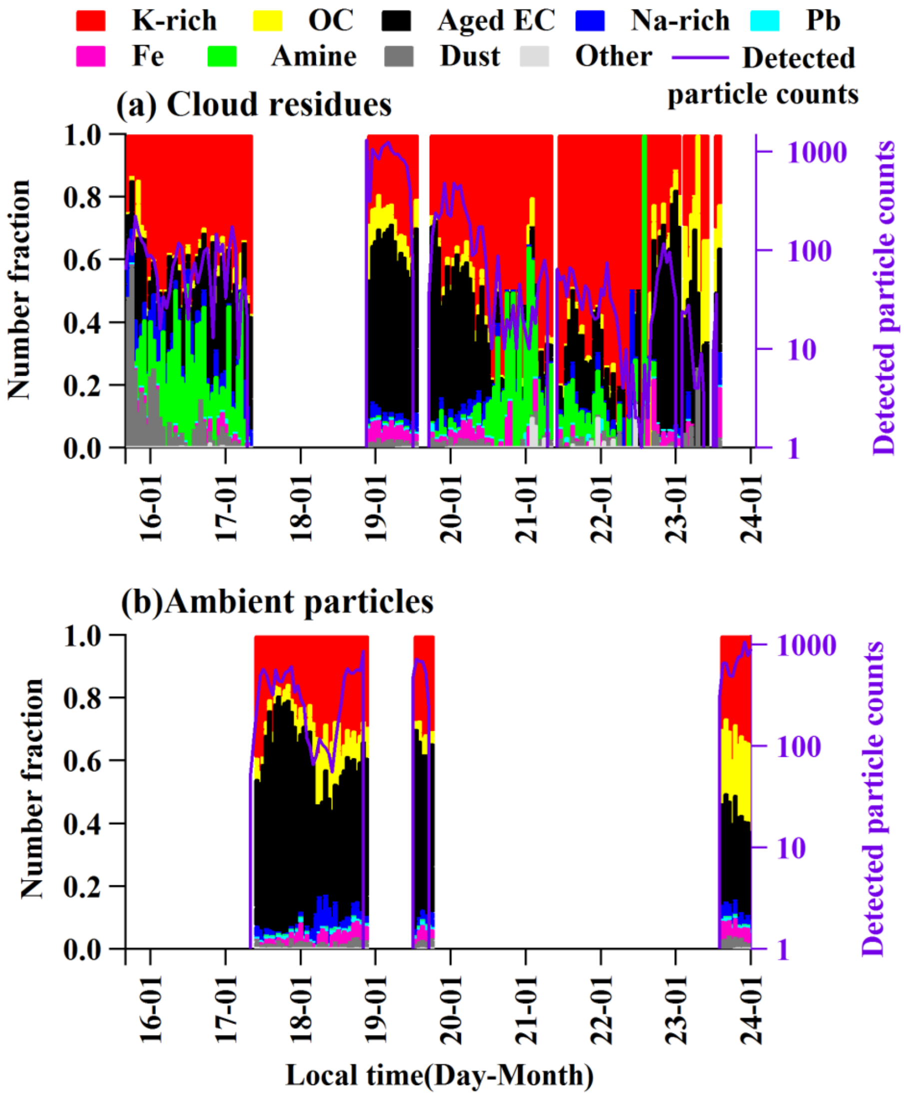

Figure 6: The hourly average variations in the cloud residual and ambient particles during the whole sampling period.

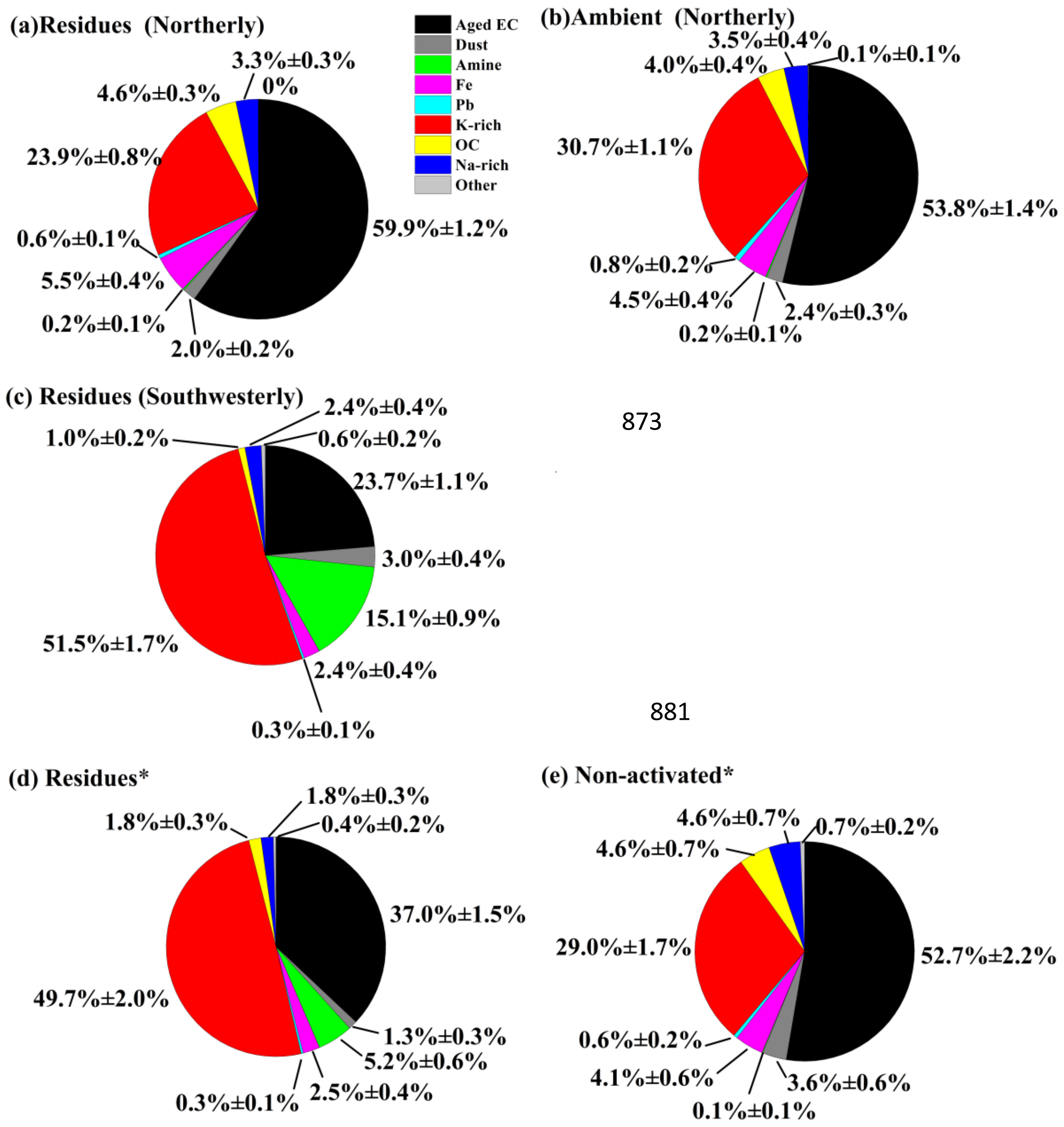

Figure 7: Number fraction of the cloud residues, ambient and non-activated particles. (a) cloud residues during northerly air mass; (b) ambient particle during northerly air mass; (c) cloud residues during southwesterly air mass; (d) cloud residues and (e) non-activated particles were alternately sampled with interval of one hour during the cloud III event; Uncertainties were calculated assuming Poisson statistics for analyzed particles.

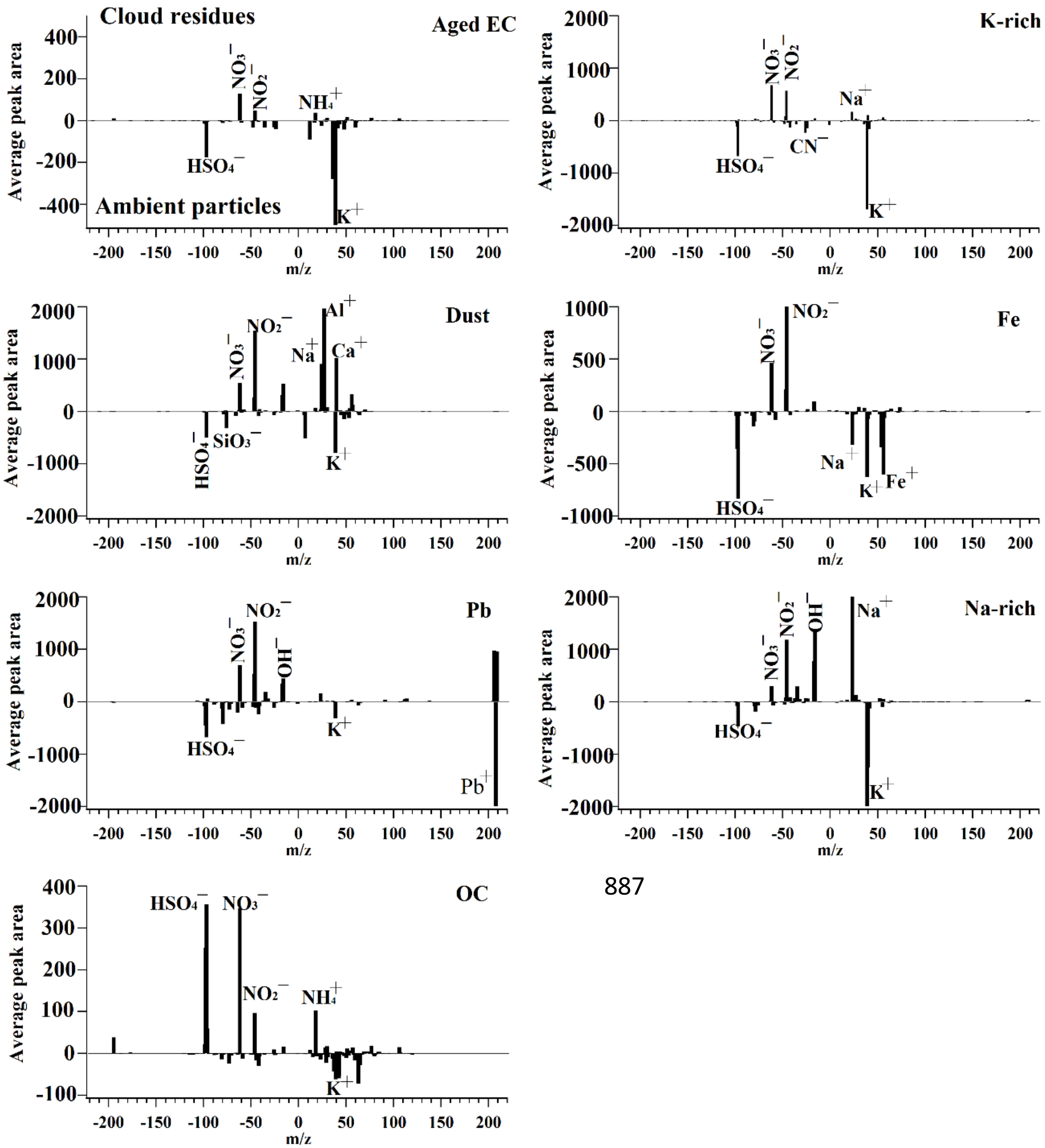

Figure 8: Mass spectral subtraction plot of the average mass spectrum corresponding to cloud residues minus ambient particles. Positive area peaks correspond to higher abundance in cloud residues, whereas negative area peaks show higher intensity in ambient particles.

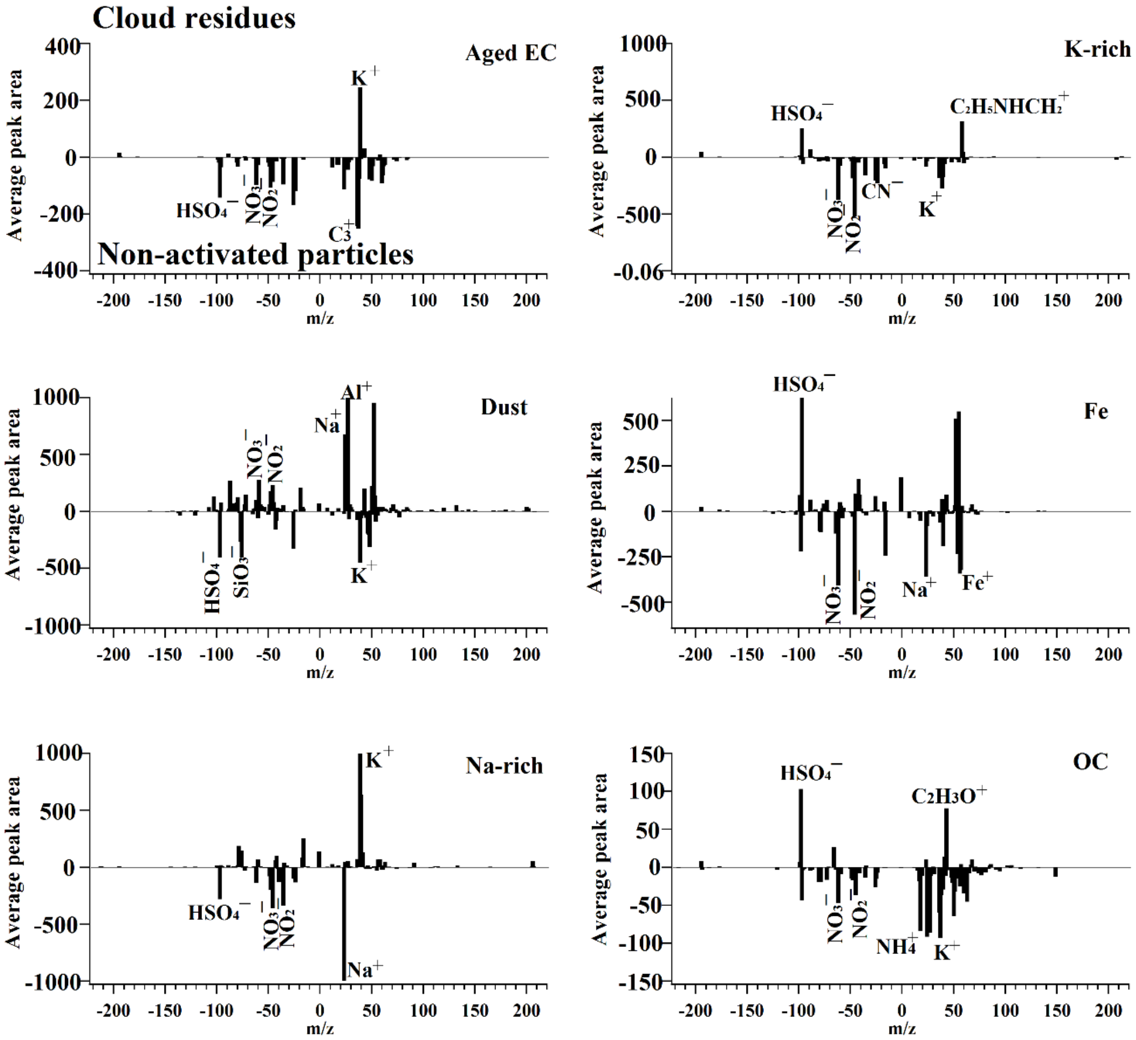

Figure 9: Mass spectral subtraction plot of the average mass spectrum corresponding to cloud residues minus non-activated particles. Positive area peaks correspond to higher abundance in cloud residues, whereas negative area peaks show higher intensity in non-activated particles.